Proceedings of the ASME 2018 37th International Conference on Ocean, Offshore and Arctic Engineering
OMAE2018
June 17-22, 2018, Madrid, Spain

OMAE2018-78326

A 2D EXPERIMENTAL AND NUMERICAL STUDY OF MOONPOOLS WITH RECESS

Senthuran Ravinthrakumar *
Department of Marine Technology
NTNU
Trondheim, Norway
E-mail: senthuran.ravinthrakumar@ntnu.no

Trygve Kristiansen
Department of Marine Technology
NTNU
Trondheim, Norway

Babak Ommani[a,b]
[a]SINTEF Ocean
Trondheim, Norway
[b]NTNU AMOS
Trondheim, Norway

ABSTRACT

Moonpool resonance is investigated in a two-dimensional setting in terms of regular, forced heave motions of a model with moonpool with different rectangular-shaped recess configurations. A recess is a reduced draft zone in the moonpool. Dedicated experiments were carried out. The model consisted of two boxes of 40 cm width each, with a distance of 20 cm between them. Recess configurations varying between 5 cm to 10 cm in length and 5 cm in height were tested. Different drafts were also tested. The free-surface elevation inside the moonpool was measured at eight locations.

A large number of forcing periods, and five forcing amplitudes were tested. A time-domain Boundary Element Method (BEM) code based on linear potential flow theory was implemented to investigate the resonance periods, mode shapes as well as the moonpool response as predicted by (linear) potential flow theory. Dominant physical effects were discussed, in particular damping due to flow separation from the sharp corners of the moonpool inlet and recess. The effect of the recess on the piston-mode behavior is discussed. BEM simulations where the effect of flow separation is empirically modelled were also conducted.

The non-dimensional moonpool response suggests strong viscous damping at piston-mode resonance. The viscous BEM simulations demonstrate improvement over inviscid BEM, although further improvement of the method is needed. The piston mode shapes are clearly different from the near flat free-surface elevation for a moonpool without recess, consistent with recently published theory.

NOMENCLATURE

η_3	Heave motion
η_{3a}	Heave oscillation amplitude
$\boldsymbol{\Omega}$	Computational domain
ϕ	Velocity potential
ρ	Density of water
ζ	Free-surface elevation
ζ_a	Free-surface elevation amplitude (basic harmonic)
D	Model draft
g	Gravitational constant
H_r	Height of recess
K	Pressure-drop coefficient
L_r	Length of recess
$\boldsymbol{n}$	Normal vector
Q	Mass flow rate
S	Surface in computational domain
t	Time variable
T_N	Natural period
$\boldsymbol{V}$	Body velocity vector
w	Vertical water particle velocity (z-direction)

INTRODUCTION

The use of moonpools offers an alternative to off-the-side operations. The advantage is that operations can take place in a sheltered deck area. A disadvantage is resonant motion in the moonpool, which occurs at certain wave periods. The highest natural period, which is for the so-called piston-mode resonance, is typically 6-8 seconds, corresponding to typical operational

*Address all correspondence to this author.

conditions. Large vertical oscillatory motion of the water occurs at piston-mode resonance. This is a significant limiting factor for operability. The traditional moonpools, referred to as clean moonpools in this paper, have been studied in forced heave and in floating conditions exposed to incoming waves over the recent years, see e.g. Kristiansen [1] and Fredriksen [2].

More recently, there exist other types of moonpools, used for instance in drilling vessels, which involves recesses. A recess is a finite water depth zone in the moonpool, used for instance as a wet working deck to float structures into the main part of the moonpool. The recess geometry affects the flow characteristics. At piston-mode resonance in moonpools with recess, the massive flux of water may lead to violent free-surface motions, introducing even stronger operational limitations.

At resonance, the amplitude of the water column is significantly over-predicted by potential flow theory, since the effect of flow seperation is not accounted for. Flow separation leads to generation of vortices. These will act at damping on the elevation of the water column inside the moonpool (Kristiansen [3]). The importance of this for moonpools with a recess is one main effect to be investigated in this work. In addition, sudden change of moonpool cross section, for instance in presence of a object, or recess in the present study, adds to the complexity of the flow. Such complexities include, blockage effect, change of moonpool natural period based on shape and location of the obstacle (Kristiansen et al. [4]), and complex flow patterns when the part of the object becomes dry (Ommani et al. [5]).

Molin [6] used domain-decomposition assuming linear potential flow theory for determining the natural periods for the piston and sloshing modes of resonance in clean moonpools. Recently, Molin [7] developed methods for determing the natural periods for moonpool configurations with recess. The methods predict mode shapes and corresponding natural periods, but not the response of the water column. Son et. Al. [8] studied moonpools with recess under forward speed conditions. They studied the increased drag on the vessel as a consequence of the moonpool, suggesting solutions for decreasing the resistance. Guo et al. [9] performed experimental and numerical studies on the response of the water column under operational conditions at varying heading angles of the incoming waves for moonpools with recess.

We start with a brief presentation of the theory of the boundary element method, and discuss main parameters of the numerical simulations. This is followed by a description of the experimental set-up. Experimental error sources are discussed. Finally, numerical and experimental results are presented in terms of amplitude-dependent response amplitude operators, mode shapes, and time-series. Although the forcing period range in the experiments includes sloshing modes, the present study includes the piston-mode only. Main findings include dominant viscous damping, mode shapes, and applicability of empirically determined viscous damping applied in BEM simulations assuming linear potential flow theory, at piston-mode resonance for moonpool configurations with recess.

NUMERICAL METHOD

We assume linear potential flow theory. The boundary value problem is given in (1), cf. also Figure 1.

$$\nabla^2\phi = 0, \qquad \text{in } \mathbf{\Omega} \tag{1a}$$

$$\frac{\partial\phi}{\partial n} = 0, \qquad \text{on } S_w \tag{1b}$$

$$\frac{\partial\phi}{\partial n} = \boldsymbol{V}\cdot\boldsymbol{n}, \qquad \text{on } S_B \tag{1c}$$

$$\frac{\partial\zeta}{\partial t} = \frac{\partial\phi}{\partial z} = w, \qquad \text{on } S_F \tag{1d}$$

$$\frac{\partial\phi}{\partial t} = -g\zeta. \qquad \text{on } S_F \tag{1e}$$

Here, ϕ and ζ are the velocity potential and free-surface elevation, respectively. $\boldsymbol{n}$ and $\boldsymbol{V}$ are the normal and body velocity vectors, respectively.

Linear BEM

The numerical studies carried out in this paper are based on the Boundary Element Method (BEM). The solution is time-stepped using a Runge-Kutta fourth-order scheme for the kinematic and dynamic free-surface conditions (1d) and (1e). The BEM formulation is well discussed in the literature, see e.g. Faltinsen and Timokha [10], which can be described as a distribution of sources and dipoles (Rankine singularities) on the surfaces enclosing the computational domain,

$$\alpha\phi = -\int_S \psi\frac{\partial\phi}{\partial n}dS + \int_S \phi\frac{\partial\psi}{\partial n}dS, \tag{2}$$

where $S = S_W + S_F + S_B$ (cf. Fig. 1), $S_F = S_{F,moon} + S_{F,out}$, $\psi = \log(r)$ and $\alpha = \pi$ on flat surfaces.

A lowest-order method is applied, i.e. the source and dipole strengths are constant over each panel. A linear equation system is established on the form $\boldsymbol{Ax} = \boldsymbol{B}$, where $\boldsymbol{x}$ consists of ϕ and $\frac{\partial\phi}{\partial n}$ on Neuman and Dirichlet boundaries, respectively. The first term on the right-hand-side in (2) must be understood as a principle value integral, due to the singularity located at the collocation points.

Numerical beaches were implemented at the ends of the tank, to avoid reflected waves from the tank ends, by introducing artificial dissipation in the kinematic and dynamic free-surface conditions,

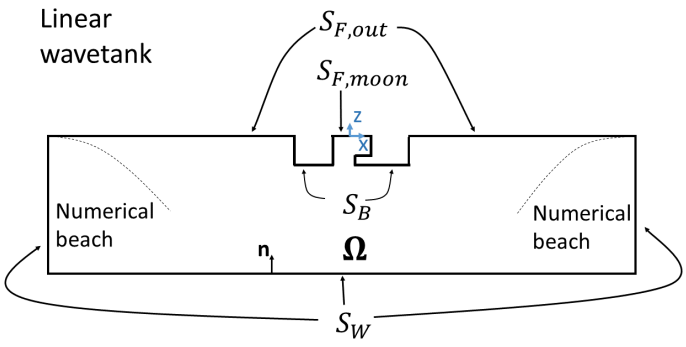

FIGURE 1. NUMERICAL WAVE TANK FOR BEM SIMULATIONS. NUMERICAL BEACHES ARE INDICATED BY DASHED LINES, BUT ARE NOT A PART OF THE MESH ITSELF.

$$\frac{\partial \zeta}{\partial t} = \frac{\partial \phi}{\partial z} - \nu_1(x)\zeta, \qquad \text{on } S_F \tag{3a}$$

$$\frac{\partial \phi}{\partial t} = -g\zeta - \nu_2(x)\phi, \qquad \text{on } S_F \tag{3b}$$

where $\nu_1(x)$ and $\nu_2(x)$ are third-order polynomials in the longitudinal direction, and their magnitudes are empirically determined.

A total of approximately 3000 panels were used in the present simulations, where 150 of them represent $S_{F,moon}$. Simulations were also performed with half as many panels, without having any noticable influence on the results. The number of time-steps per period is 120, and each simulation is run for approximately 60 periods. The CPU time was approximately 120 s on a single 3.6 GHz CPU for a simulation with 60 periods.

Viscous Effects in BEM

The damping due to flow separation at the moonpool inlet is modelled in the present linear BEM model by means of a pressure drop coefficient, as presented by Faltinsen and Timokha [11]. The flow separation at the inlet is associated with a pressure drop. Faltinsen and Timokha [11] exploided this fact by assuming that mirroring of the set-up mimics a slat screen. They transfer the drop in pressure, which in reality occurs in relation to the inlet, to the dynamic free-surface condition. The drop in pressure is expressed as $\Delta p_{moonpool} = 0.5\Delta p = \frac{1}{4}\rho K \overline{w}|\overline{w}|$, where K is unknown a priori, and is a function of solidity ratio and KC (Keulegan-Carpenter) number. In [11] and the present study, it is assumed that K is independent of the KC-number. Δp is the pressure drop for a slat screen, and $\Delta p_{moonpool}$ is the pressure drop experienced in the moonpool.

In [11] $\overline{w}$ is the averaged velocity at the inlet. However, there is a slight phase difference between the velocities at the inlet and the free-surface when there is a recess. Therefore, $\overline{w}$ has been modified to be the averaged velocity at the free-surface (cf. (4)) in the present study, since the free-surface elevation is directly related to the vertical velocity at the free-surface by the kinematic free-surface condition (1d),

$$\overline{w} = \frac{1}{L}\int_L w\, dx \qquad \text{on } S_{F,moon} \tag{4}$$

where L is the length of the gap at the still waterline, and w given by (1d). Thus, (3b) becomes

$$\frac{\partial \phi}{\partial t} = \begin{cases} -g\zeta - \nu_2(x)\phi - \frac{1}{4}K(\mathrm{Sn})\overline{w}|\overline{w}| & \text{on } S_{F,moon} \\ -g\zeta - \nu_2(x)\phi & \text{on } S_{F,out} \end{cases} \tag{5}$$

on the free-surface ($z = 0$), S_F. The kinematic free-surface condition remains (3a).

The pressure-drop coefficient is, according to [11], calculated as

$$K(\mathrm{Sn}) = \left(\frac{1}{C_0(1-\mathrm{Sn})} - 1\right)^2,\ C_0 = 0.405\exp(-\pi \mathrm{Sn}) + 0.595 \tag{6}$$

Here Sn is the solidity ratio of the mirrored geometry as discussed in [11], and C_0 is the so-called contraction coefficient.

EXPERIMENTAL SET-UP

Dedicated experiments were carried out in the period August to October 2017 in a glass wall wave flume at the Marine Technology Center in Trondheim. The tank is 13.5 m long and 0.6 m wide (Fig. 2). The water depth in the tank was varied between 95 cm - 105 cm. It is equipped with two parabolic beaches, one on each side, in order to avoid reflected waves from the tank ends. Two boxes with the dimensions 40 cm $\times$ 59 cm $\times$ 40 cm were rigidly connected 20 cm apart to represent a moonpool configuration, where various recess configurations were tested (Figs. 3 and 4). The draft of the model was varied to study the effect of water depth over the recess. The resonant fluid motion at both piston and sloshing modes were studied.

In the present study, the focus is the piston-mode resonance. About 20 configurations were tested, where four representative cases are chosen for the present paper (see Table 1). A photo of Case 4 is shown in Figure 5. The model was forced to heave with specified amplitudes and periods. The forced heave amplitude, η_{3a}, was varied between 1 mm - 5 mm, with a step of 1 mm. The step size of the forcing periods, T, was approximately 0.05 s, and was refined to approximately 0.01 s around resonance of the water column. The model tests were automated in the sense that a long time-series (typically 24 hours) was given as input to the oscillator. The time-series consisted of a range of sinusoidal

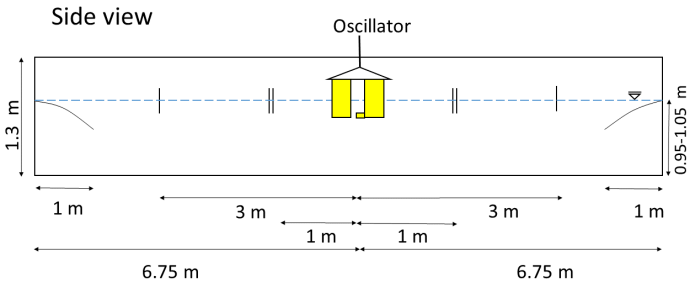

FIGURE 2. SIDE VIEW OF THE EXPERIMENTAL SET-UP, SHOWING THE LOCATION OF THE PARABOLIC BEACHES AND WAVE PROBES OUTSIDE THE MOONPOOL.

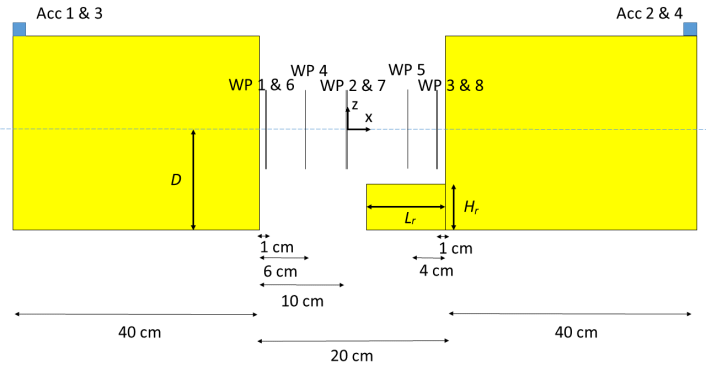

FIGURE 3. LOCATIONS OF THE WAVE PROBES (WP) INSIDE THE MOONPOOL, AND ACCELEROMETERS (ACC).

signals with varying oscillation amplitudes and periods, in addition to a resting time for the free-surface in the tank to become calm. This facilitated efficient model tests. Typically, 400 - 500 tests were achieved in a 24 hour duration run.

Eight wave probes of capacitance type were used to measure the free-surface elevation in the moonpool, as shown in Figure 4. Six of them were paired together, such that possible transverse sloshing could be identified. This means that water elevation was measured at five different locations in the longitudinal direction in the moonpool. Six wave probes of capacitance type were used outside the moonpool, mainly to check any evidence of reflected waves and transverse sloshing in the wave flume (four of them were paired).

Forces were measured in the vertical and horizontal direction (x- and z-direction) with a force transducer. Forces are, however, not presented in the present paper. The vertical model position was measured by means of a displacement sensor. In addition, six accelerometers were used to measure accelerations in x-, y- and z- directions. Four of them (Acc 3-6) were used to verify that pure vertical motions were obtained by measuring accelerations in the horizontal plane, while the remaining two (Acc

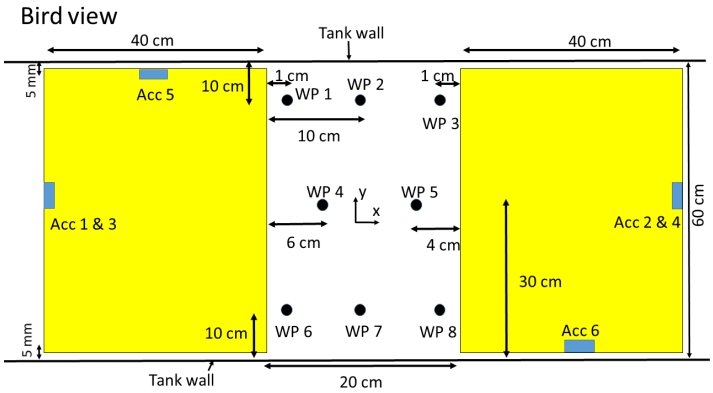

FIGURE 4. BIRD VIEW OF THE WAVE PROBES (WP) INSIDE THE MOONPOOL, AND ACCELEROMETERS (ACC).

FIGURE 5. EXPERIMENTAL CONFIGURATION (CASE 4) WITH RECESS DIMENSIONS 10 cm $\times$ 5 cm (20 cm AT THE WATERLINE).

1 and 2) were used for measuring accelerations in z-direction, in addition to validate motions determined by the position sensor. The locations of the accelerometers are shown in Figures 3 and 4. All measurements in the experiments were logged at 200 Hz.

Parabolic Beaches

The tank is equipped with two parabolic beaches; one on each side of the tank to avoid reflected waves. With a parabolic beach, however, it is not always possible to avoid reflection for all wave periods and wave steepnesses. For long waves ($T > 1.4$ - 1.5 s), some reflection was expected. The parabolic beaches were adjusted prior to each experimental program such that the top of the beaches are located approximately 2 mm below the free-surface, which was found in Kristiansen and Faltinsen [1] to

TABLE 1. TEST CASES IN THE PRESENT EXPERIMENTS

Case	Draft (D)	Recess dimensions ($L_r \times H_r$)
Case 1	11.5 cm	5 cm × 5 cm
Case 2	11.5 cm	7.5 cm × 5 cm
Case 3	15.0 cm	5 cm × 5 cm
Case 4	11.5 cm	10 cm × 5 cm

be efficient for absorbing waves with small wave steepness.

Error Analysis in Model Tests

The model tests were conducted carefully in order to minimize inaccuracies and errors in the measurements. However, possible bias and random errors should be addressed to discuss the quality of the experimental results.

Wave Probes It is known from experience that the calibration factor of the wave probes are temperature dependent. Even though the currently used wave probes are supposed to correct for this error, a small deviation for large temperature variations in the water surrounding the gauges might have an impact on the results. The temperature variations were, however, relatively small during the testing period.

As most of the traditional equipment used for measurement, the wave probes might drift over time. This offset was accounted for by daily zero-setting, and during post-processing. The paired wave probes gave very similar results except when transverse sloshing occured.

Transverse Sloshing Transverse sloshing might be induced inside the moonpool. Both video recordings and wave elevation measurements were used to identify possible transverse sloshing. No transverse sloshing was registered in the range of forcing periods presented in this present study. Transverse sloshing in the moonpool typically did, however, occur between $T =$ 0.7 - 1.0 s, depending on the draft and recess length.

The first transverse sloshing mode of the wave flume can be calculated to be approximately 0.88 s as shown in Faltinsen and Timokha [10], which is outside the range of periods presented in this paper. The first longitudinal sloshing (seiching) mode for the tank can be found to be approximately 8.7 s, which is far outside the range tested in the present tests.

Distance between Glass Walls and Model A distance of 5 mm was used between the model and the glass walls of the tank, in order to avoid contact between them. This allows the water to flow in and out between the model and wall, which ultimately introduces a 3D effect. This gap is, however, not more than 1.67 % of the total width of the tank and in addition, the flow is dominated by boundary layers, so the mass flux of water in and out of the gap is small.

Repeatability In order to check for evidence of random errors, selected cases were repeated eight times. The response amplitude operators (RAOs) and time-series correspond well. In the range studied in this paper work, the largest difference in the RAO is less than 2 %.

Accelerometers versus Position Sensor The position measurements are made with a metallic wire which is displaced along with the oscillator. Acceleration measurements in the vertical direction are integrated twice in time in order to obtain the vertical position. This corresponds well to that measured by the displacement sensor. In general, differences less than 1.5% were observed. In some occasions, the displacement sensor failed. Consequently, accelerometers are used for determining the heave motion, η_3, in the present study.

General Observations Video recordings of the model tests were performed with a single-lens reflex (SLR) camera. Observations made visually and with video recordings suggest highly non-linear and violent free-surface flow at the natural sloshing frequencies. In particular, large forcing amplitudes at the first sloshing mode induced strongly non-linear flow. These results are not considered in the present study. Violent flow at the piston-mode resonance was not observed, even though the response at the piston-mode is relatively large. No secondary resonant modes were excited around the piston-mode.

RESULTS

Results from the numerical simulations with linear BEM and experiments are compared in this section. Numerical results for the free-surface elevation are extracted at the same locations as in the experiments. Amplitude-dependent RAOs of the free-surface are presented, along with mode shapes and time-series. BEM results both with and without empirical damping are presented.

Natural Periods

In Molin [7] an approximation for the piston-mode natural frequency in a moonpool with recess is obtained by assuming that the water inside the moonpool can be assumed as a solid body, giving an equation of motion as

$$\left(\rho ad + M_{al} + M_{au}(\omega)\right)\ddot{\zeta} + \rho g \frac{a^2}{L}\zeta = 0, \tag{7}$$

TABLE 2. NATURAL PERIOD FOR THE PISTON MODE

Case	T_N from [7]	T_N from BEM
Case 1	1.18 s	1.19 s
Case 2	1.25 s	1.26 s
Case 3	1.22 s	1.24 s
Case 4	1.35 s	1.35 s

where the term proportional to $\ddot{\zeta}$ is mass and added mass of the water column, while the term proportional to ζ represents the water plane stiffness. ζ is the free-surface elevation. a, d and L are length of opening at inlet, height of recess and length of moonpool opening at still waterline, respectively (cf. Figure 16). M_{al} and M_{au} are added mass for the lower and upper fluid domain as found in [7], respectively. There, the flow is assumed to be two-dimensional in the moonpool, and three-dimensional outside. Moreover, infinite water depth is assumed. In the present estimation of the natural periods, M_{al} has been modified to account for the fact that the flow is two-dimensional and the finite water depth in the tank (see Appendix A). The predicted natural periods for the piston-mode, T_N, are presented in Table 2, along with the natural periods determined by the present BEM simulations.

Time-Series - Examples

Experimentally measured and numerically calculated time-series of the wave elevation inside the moonpool are presented for Case 1 and Case 4 in Figure 6. The results are for forcing periods at $T = 1.2$ s and $T = 1.35$ s for Case 1 and Case 4, respectively. The oscillation amplitudes are 1 mm and 5 mm. Steady state is obtained in both the experiments and the numerical simulations within 10-15 oscillation periods. A linear ramp up and ramp down of five periods are used at the beginning and end of the time-series.

Response Amplitudes Operators

Amplitude-dependent Response Amplitude Operators (RAOs) are created for the free-surface elevation inside the moonpool. Figures 7 and 8 show that the natural periods are predicted well by the BEM. Further, it is observed that $\frac{\zeta_a}{\eta_{3a}}$ decreases with increasing amplitude of motion. This clearly shows that damping due to flow separation at sharp corners is of major importance at the piston-mode resonance, also in the presently studied cases with recess, as for clean moonpools. The numerical and experimental results compare well outside the region of resonance, as expected, since damping plays a less

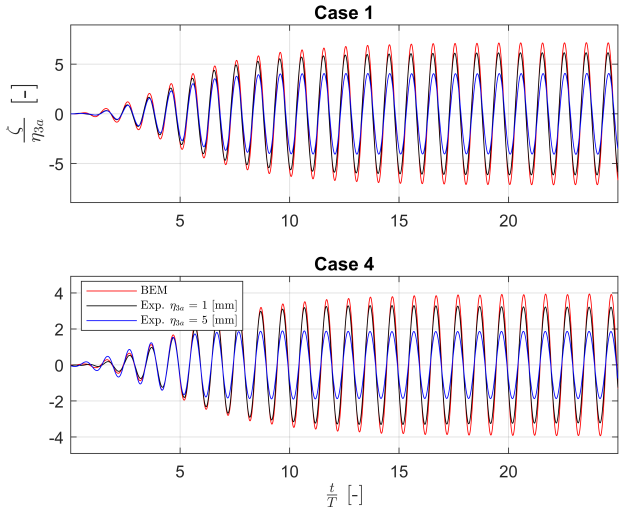

FIGURE 6. TIME-SERIES FOR *WAVE PROBE 1* IN MOONPOOL. $T = 1.2$ s FOR CASE 1 AND $T = 1.35$ s FOR CASE 4. EXP.: EXPERIMENTAL VALUES.

significant role away from resonance, and the response will be mass and stiffness dominated.

The magnitude of the response in the RAOs decrease with increasing recess length. This is mainly due to decreased ratio between the inlet width and gap width at the still waterline. Since the particle velocity at resonance is lower due to the shift in the natural period, as shown in Figure 9, the mass flux through the moonpool decreases. The viscous damping, which is quadratic in the relative velocity between the flow and body, is however higher for cases with larger recess and draft (cf. Table 3). This could intepreted as an increase in the drag coefficient due to the increase in the recess length (drag coefficient in relation to the viscous damping of the free-surface elevaiton in the moonpool).

The natural period increases with increasing recess length. The free-surface elevation inside the moonpool can be thought upon as a mass-spring system as shown in (7). The presence of the recess has the effect of increasing the added mass of the water column.

Mode Shapes for Piston Mode Resonance

The mode shape is nearly uniform for a clean moonpool. For a moonpool with a recess, however, the mode shape has a non-negligible variation across the moonpool, with the largest value at the recess end wall. At the opposite wall, the free-surface elevation is at its minimum. This behavior is captured both by the numerical BEM results, and the present experiments. The mode shapes predicted by BEM are compared to experimental results for Case 4 in Figure 10. For clean moonpools the free-surface amplitude is largest at the middle of the opening, with a slight

TABLE 3. DIFFERENCE BETWEEN RESPONSE FROM BEM AND EXPERIMENTS ($\eta_{3a} = 1\ mm$) AT RESONANCE

Case	Difference in %
Case 1	25.7
Case 2	31.1
Case 3	35.3
Case 4	33.0

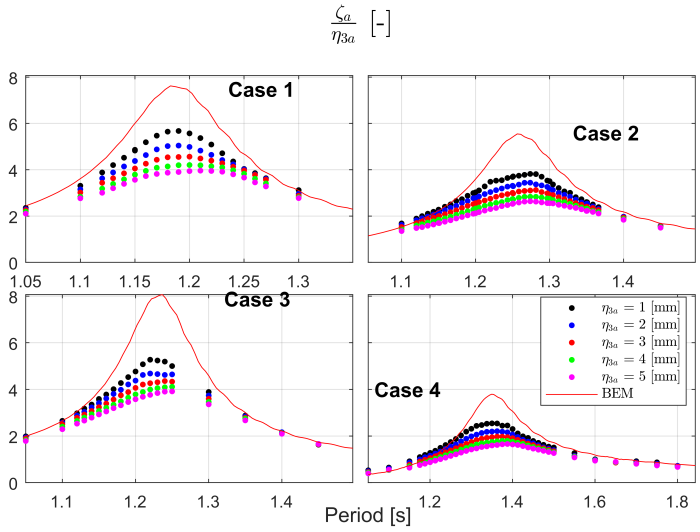

FIGURE 7. RAO FOR ALL CASES, BOTH NUMERICAL AND EXPERIMENTAL RESULTS. ZOOMED IN AROUND THE PISTON MODE RESONANCE FOR *WAVE PROBE 1* IN MOONPOOL.

decrease towards the walls. This is discussed e.g. in Molin [6], where it is illustrated that the ratio of the free-surface elevation at the center and ends is dependent on the beam-to-draft ratio in the moonpool.

The ratio between the free-surface elevation at the recess end and the center or the opposite wall end increases with decreasing draft in the moonpool. The same tendency is observed for increasing length of the recess. The present results are consistent with [7]. The increase of the free-surface elevation at the recess end is there discussed, and the study shows that the shallower the zone in the recess becomes, the more prominent the difference in the free-surface elevation at the recess end and opposite end becomes. For the present four cases, the effect is illustrated in Figure 11. Case 1 and 3 have the same horizontal dimensions, while the draft is larger for Case 3. The mode shape has slightly less variation with increasing draft.

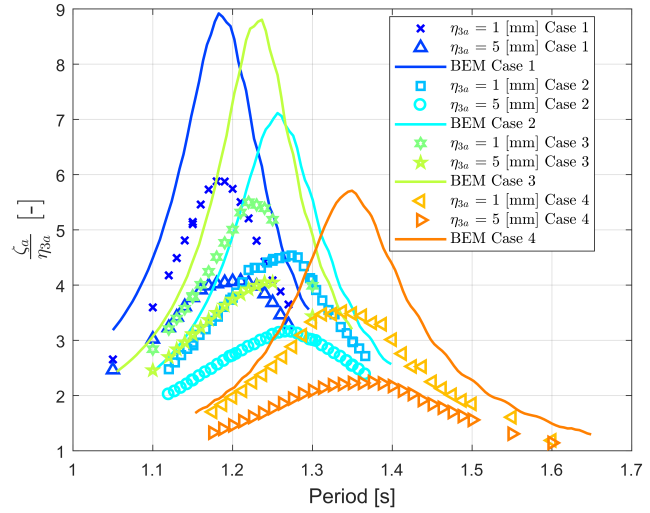

FIGURE 8. RAO FOR ALL CASES, BOTH NUMERICAL AND EXPERIMENTAL RESULTS AROUND THE PISTON MODE FOR *WAVE PROBE 8* IN MOONPOOL.

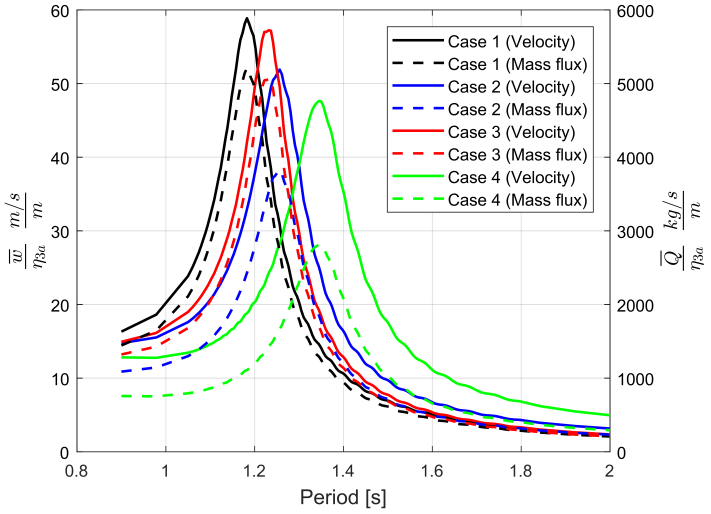

FIGURE 9. RAO FOR AVERAGED PARTICLE VELOCITY AND AVERAGED MASS FLUX THROUGH INLET FROM BEM SIMULATIONS. $\overline{w}$ AND $\overline{Q}$ ARE AVERAGED VERTICAL VELOCITY AND MASS FLOW RATE AT INLET.

BEM with Viscous Damping

Figures 12-15 present the results from the BEM simulations accounting for the effect of flow seperation assuming that the moonpool geometry can be associated by a slat screen, as discussed in relation to (4) - (5). In general, these results represent a clear improvement relative to BEM without accounting for the

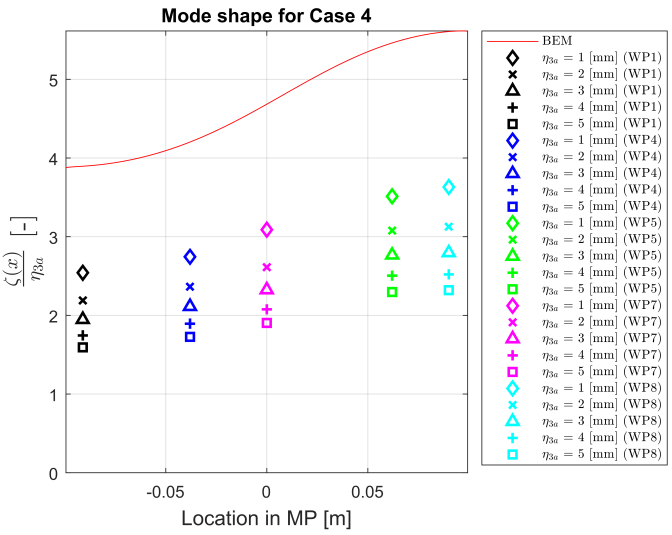

FIGURE 10. MODE SHAPES FOR CASE 4 WITH EXPERIMENTAL DATA IN MOONPOOL (MP) FOR $T = 1.35$ s.

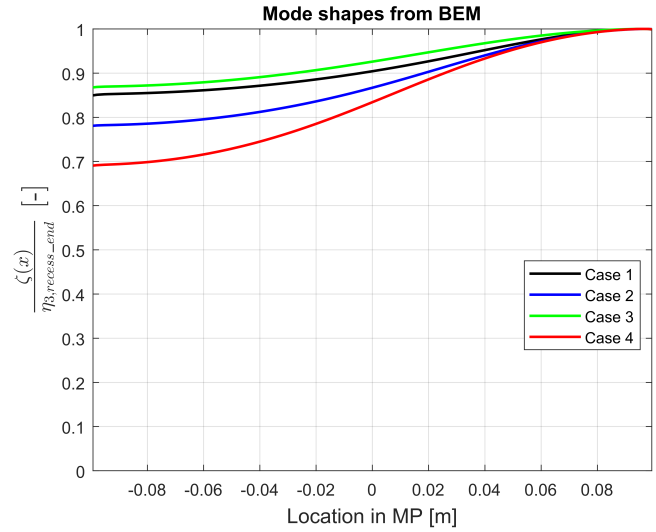

FIGURE 11. MODE SHAPES AT PISTON MODE RESONANCE AS PREDICTED BY PRESENT BEM SIMULATIONS.

additional damping due to flow separation at the moonpool inlet, although improvement of the proposed empirical method should be made in future studies in order to obtain even better comparisons. The results for BEM accounting for viscous damping compare best for Case 2, which has a smaller recess than Case 4 (i.e. the method yields best comparison for cases with smaller recess).

The deviations for Case 4 are larger near the recess wall than the opposite wall (cf. Figures 14 and 15). Since an averaged free-

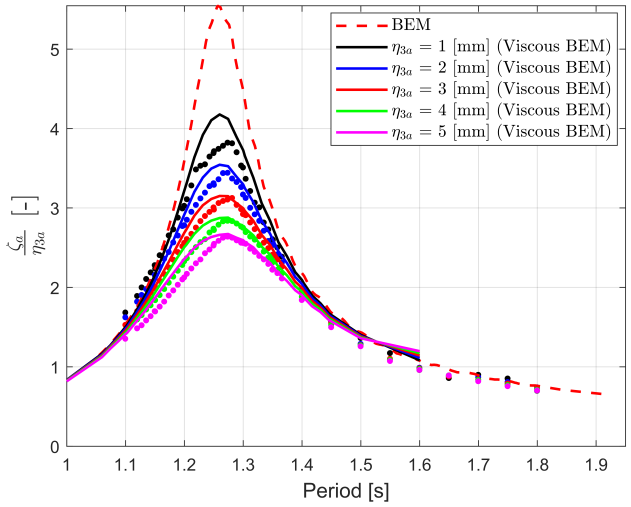

FIGURE 12. RAO FOR VISCOUS BEM SIMULATIONS VERSUS EXPERIMENTAL RESULTS FOR CASE 2 (*WAVE PROBE 1*). DOTS INDICATE EXPERIMENTAL DATA.

surface velocity is used in (5), the large free-surface elevation at the recess end is not damped as much as at other locations along the free-surface in the moonpool. The most pronounced variation in the mode shape is noticed for Case 4, where the largest discrepancy in the RAO with viscous BEM is noticed. Increasing the pressure-drop coefficient might improve the results at the recess wall end, but is also likely to give non-conservative results e.g. at the opposite wall end or center of moonpool.

CONCLUSION

The piston-type resonance of moonpools with recess was studied experimentally and numerically in a two-dimensional setting. Dedicated two-dimensional experiments were carried out in a wave flume at the Marine Technology Center in Trondheim. An automatic test program to perform tests with a large range of periods and oscillation amplitudes was used. The test range included both sloshing and piston-mode resonance. At sloshing, severe non-linear free-surface behavior was observed. However, at piston-mode, discussed herein, the behavior was not violent. A linear time-domain BEM code was implemented in order to study the problem numerically. Numerical simulations assuming potential flow theory over-predict the moonpool response at resonance.

The importance of viscous damping around piston-mode resonance is pointed out by performing experiments at varying amplitudes of oscillation. The amplitude-dependent RAOs show that the viscous effects due to flow seperation at the inlet of the moonpool has a dominant effect at resonance, similar to that for moonpools without recess.

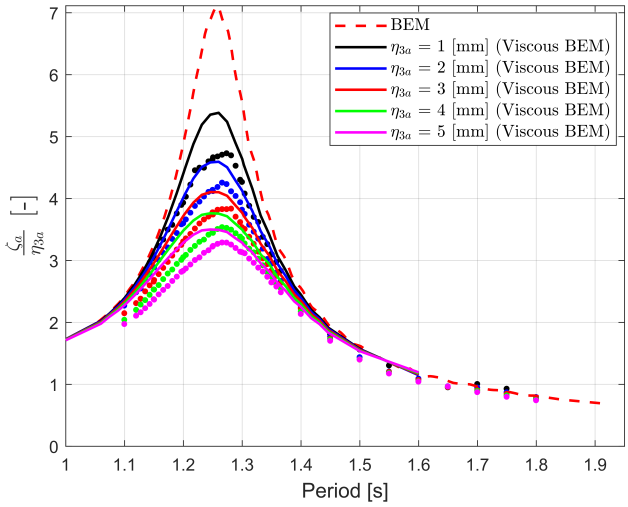

FIGURE 13. RAO FOR VISCOUS BEM SIMULATIONS VERSUS EXPERIMENTAL RESULTS FOR CASE 2 (*WAVE PROBE 8*). DOTS INDICATE EXPERIMENTAL DATA.

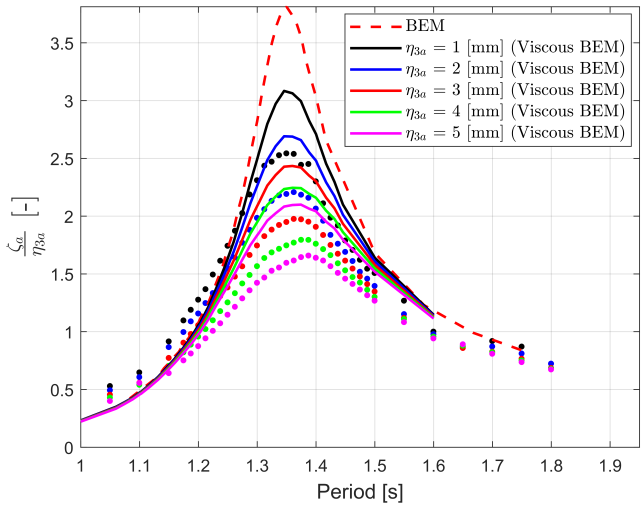

FIGURE 14. RAO FOR VISCOUS BEM SIMULATIONS VERSUS EXPERIMENTAL RESULTS FOR CASE 4 (*WAVE PROBE 1*). DOTS INDICATE EXPERIMENTAL DATA.

The free-surface elevation at the recess end is largest. This effect was predicted both by the present experiments and BEM simulations. This phenomenon becomes more prominent with increasing recess dimensions and decreasing water depth above recess in the moonpool. The mode shapes for moonpools with recess are therefore seen to be different than for the ones for a clean moonpool, consistent with recent theory by Molin [7].

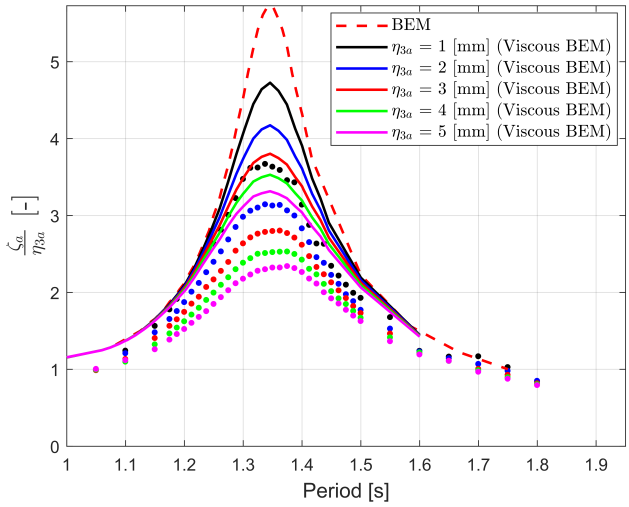

FIGURE 15. RAO FOR VISCOUS BEM SIMULATIONS VERSUS EXPERIMENTAL RESULTS FOR CASE 4 (*WAVE PROBE 8*). DOTS INDICATE EXPERIMENTAL DATA.

Simulations where viscous effects are accounted for in an empirical manner in the BEM simulations. The pressure drop due to flow separation at the moonpool inlet is accounted for by assuming that the moonpool configuration can be presented by a screen, as discussed in Faltinsen and Timokha [11]. In the present study, the averaged velocity at the inlet, used in the expression for the pressure drop, is replaced by the average velocity at the free-surface. The results from the viscous BEM simulations represent a clear improvement relative to those without. At the recess end, however, considerable deviation from the experimental data is noticed. This is probably due to the non-uniform variation of the free-surface in cases with a large recess. The method shows promising results, and deserve future attention for improvement.

ACKNOWLEDGMENT

The authors would like to thank professor O.M. Faltinsen and professor B. Molin for valuable discussions.

REFERENCES

[1] Kristiansen, T., and Faltinsen, O. M., 2012. "Gap resonance analyzed by a new domain-decomposition method combining potential and viscous flow draft". *Applied Ocean Research,* ***34***, pp. 198–208.

[2] Fredriksen, A. G., Kristiansen, T., and Faltinsen, O. M., 2015. "Wave-induced response of a floating two-dimensional body with a moonpool". *Phil. Trans. R. Soc. A,* ***373***(2033), p. 20140109.

[3] Kristiansen, T., 2009. "Two-dimensional numerical and experimental studies of piston-mode resonance". *PhD thesis*.
[4] Kristiansen, T., Ommani, B., Berget, K., and Baarholm, R., 2015. "An experimental and numerical investigation of a box-shaped object in moonpool: A three-dimensional study". In ASME 2015 34th International Conference on Ocean, Offshore and Arctic Engineering, American Society of Mechanical Engineers, pp. V001T01A038–V001T01A038.
[5] Ommani, B., Kristiansen, T., Berget, K., Sandvik, P., and Faltinsen, O. M., 2016. "An investigation on moonpool blockage by box-shaped object close to free surface". *International Conference on Violent Flows*.
[6] Molin, B., 2001. "On the piston and sloshing modes in moonpools". *Journal of Fluid Mechanics,* ***430***, pp. 27–50.
[7] Molin, B., 2017. "On natural modes in moonpools with recesses". *Applied Ocean Research,* ***67***, pp. 1–8.
[8] Son, H.-J., Choi, S.-H., Kim, M.-H., and Hwangbo, S.-M., 2008. "Drag reduction of recess type moonpool under vessel's forward speed". In Proc. 27th Int. Conf. on Offshore Mechanics and Arctic Engineering.
[9] Guo, X., Lu, H., Yang, J., Peng, T., et al., 2016. "Study on hydrodynamic performances of a deep-water drillship and water motions inside its rectangular moonpool". In The 26th International Ocean and Polar Engineering Conference, International Society of Offshore and Polar Engineers.
[10] Faltinsen, O. M., and Timokha, A. N., 2009. "Sloshing".
[11] Faltinsen, O., and Timokha, A., 2015. "On damping of two-dimensional piston-mode sloshing in a rectangular moonpool under forced heave motions". *Journal of Fluid Mechanics,* ***772***.

Appendix A: Modifying M_{al} in Estimation of Natural Periods

The estimation of the piston-mode natural period is achieved by means of domain decomposition, as presented in Molin [7]. In the present study, M_{al} in (7) has to be modified such that the effect of finite water depth, and the two-dimensional flow assumption outside the moonpool is accounted for. The boundary value problem is

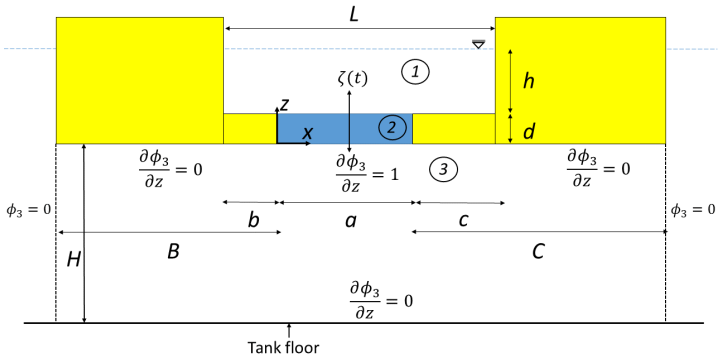

FIGURE 16. GEOMETRY OF MOONPOOL WITH RECESS ALONG WITH BOUNDARY CONDITIONS.

$$\nabla^2\phi_3 = 0, \qquad \text{in domain 3} \tag{8a}$$
$$\frac{\partial\phi_3}{\partial z} = 0, \qquad \text{on } z=-H \tag{8b}$$
$$\frac{\partial\phi_3}{\partial z} = 1, \qquad \text{on } z=0 \text{ and } 0\le x\le a \tag{8c}$$
$$\frac{\partial\phi_3}{\partial z} = 0, \qquad \text{on } z=0 \text{ and } -B\le x\le 0 \tag{8d}$$
$$\frac{\partial\phi_3}{\partial z} = 0, \qquad \text{on } z=0 \text{ and } a\le x\le a+C \tag{8e}$$

where a, B, C and H are geometric dimensions as shown in Figure 16. ϕ_3 is the velocity potential in the lower fluid domain, which gives the added mass from the lower fluid domain as shown in (11) by solving the boundary value problem. The general expression for ϕ_3 is given in (9), where it satisfies Laplace equation, no flow through the tank floor, and truncation condition at $x=-B$ and $x=a+C$.

$$\phi_3(x,z) = \sum_{n=1}^{\infty} D_n \frac{\cosh\mu_n(z+H)}{\cosh\mu_n H}\sin\mu_n(x+B) \tag{9}$$

where $\mu_n = \frac{n\pi}{a+B+C}$. In this form, all conditions except the Neumann conditions on $z=0$ are satisfied (cf. Figure 16). Satisfying the Neumann condition, multiplying both sides with $\sin\mu_m(x+B)$ and integrating over the domain of validity gives

$$D_m = \frac{-2\left[\cos(\mu_m(a+B)) - \cos(\mu_m B)\right]}{\mu_m^2\tanh(\mu_m H(a+B+C))}, \tag{10}$$

$$M_{al} = \rho\int_0^a \phi_3(x,0)dx = -\rho\sum_{n=1}^{\infty}\frac{D_n}{\mu_n}\left[\cos\left(\mu_n(a+B)\right) - \cos\left(\mu_n B\right)\right]. \tag{11}$$